ASME Journal of Engineering for Gas Turbines and Power
Online journal at:
https://asmedigitalcollection.asme.org/gasturbinespower

Integrated Design and Operation Assessment of a Preheating System for Liquid Hydrogen Fueled Engines

Pavlos Rompokos
Cranfield University,
College Road,
Wharley End,
Bedford MK43 0AL, UK
e-mail: Pavlos.rompokos@cranfield.ac.uk

Sangkeun Kang
Cranfield University,
College Road,
Wharley End,
Bedford MK43 0AL, UK
e-mail: sangkeun.kang@cranfield.ac.uk

Ioannis Roumeliotis
Cranfield University,
College Road,
Wharley End,
Bedford MK43 0AL, UK
e-mail: i.roumeliotis@cranfield.ac.uk

Cryogenic liquid hydrogen (LH_2) is highly considered as a potential long-term solution toward emissions reduction in the aviation sector. However, one of the major challenges that the handling and integration of the cryogenic fuel introduces is thermal management. In this paper, the design space exploration of an LH_2 conditioning is presented to identify potential feasible solutions and limitations for its implementation. The preheating system comprises of secondary combustor that feeds a heat exchanger with hot gases to adequately supply the main engine with gaseous hydrogen at a constant temperature. The design space exploration addresses the heat exchanger design as well as the effect of retrofitting the system on kerosene-designed engines with different specific thrust. For performing the analysis, four baseline engine models and their equivalent integrated versions with the fuel preheating system have been created. Additionally, a framework for the sizing and off-design performance characterization of the heat exchanger is introduced. The integrated system performance across the design space is analyzed and a novel control strategy of the preheating system is proposed with the view of avoiding water vapor condensation of the hot gases of the preheating module. By applying this control, it was found that heat exchanger designs with lower effectiveness are less likely to lead to water condensation conditions and can adequately be supported with air sourced from the bypass duct without significant penalty in the overall energy efficiency of the engine. [DOI: 10.1115/1.4071241]

1 Introduction

As liquid hydrogen is increasingly seen as a long-term replacement for carbon-based fuels to decarbonize aviation, one of the main challenges that its implementation introduces is thermal management. At liquid form, hydrogen is stored at cryogenic temperatures of around 20–26 K [1], and based on the fuel properties, in order to raise its temperature to, e.g., 300 K, LH_2 requires 4 MJ/kg of fuel [2].

This considerable amount of heat requirement can be accommodated utilizing engine sources. For example, proposed LH_2 conditioning configurations involve the use of air to hydrogen heat exchangers with high integration with the main gas path of the engine. These can be either intercooled [1,3] or regenerative configurations [1,4] that also enable synergistic benefits when engine and fuel system are closely designed. However, they offer limited control over the delivery temperature of hydrogen, since the performance of the heat exchangers is mainly dependent on the gas path and in extension, the power setting of the engine. Contrary to that, another solution would be to use a hydrogen preheating module like the parallel hydrogen combustion system (PHC) proposed by Refs. [5] and [6] and presented in Fig. 1. This configuration is using air bled from the engine and directs it to a secondary combustor that increases its temperature to allow for adequate heat transfer margins. The hot gases are then passed in a heat exchanger to raise the temperature of the cold hydrogen. Comparing to the configurations this solution is thermodynamically less efficient since it increases the engine's parasitic losses but may offer adequate control over the delivery conditions of H2. In addition, since it does not impose physical changes to the main gas path of the engine, it could be a fitting candidate in a retrofitting scenario.

In the scenario where aviation would gradually transition toward LH_2, it is likely that off-the-self products are to be used to power the first generation of LH_2 aircraft, as discussed by Huete et al. [7]. As such, kerosene-designed turbofans may be retrofitted to power LH_2 aircraft with similar takeoff weight characteristics but the aircraft operational capabilities will vary as demonstrated by Saias [8] and Rischmuller [9].

In a previous study conducted by the authors [10], the impact of retrofitting such a PHC system on a kerosene-designed turbofan was examined, and concluded that the least penalizing solution in terms of engine operability was to supply the PHC unit with air from the bypass duct. The analysis focused mainly on the effect of PHC integration on the engine and showcased that the bypass bleed and power off-take requirements do not significantly impact compressor surge margines. In addition, due to the turbomachinery rematching, shaft over-speeding was identified, which can then be mitigated by reconfiguring the core nozzle and the angle of the nozzle guide vanes of the high-pressure turbine.

Turbo Expo: Turbomachinery Technical Conference and Exposition (GT2025), June 16–20, 2025.
Manuscript received October 12, 2025; final manuscript received February 24, 2026; published online April 24, 2026. Editor: Jerzy T. Sawicki.

Copyright © 2026 by ASME; reuse license CC-BY 4.0

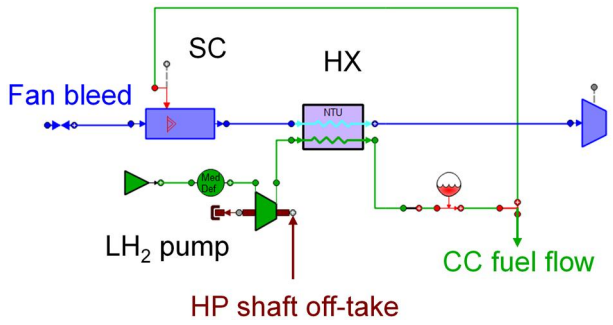


Fig. 1 PHC conditioning system

The aim of this paper is to examine in more detail the effect of the design considerations of the PHC module, and more specifically the heat exchanger, across the operating envelope of the engine. To achieve this an integrated methodology is introduced for the sizing and simulation of engine – LH_2 conditioning systems with the focus on the off-design performance of the heat exchanger of the fuel conditioning unit. In addition, a novel control strategy for the operation of the heat exchanger is proposed in order to avoid conditions that may enable water vapour condensation at the exhaust of the PHC. This is a common phenomenon occurring at the air cycle machines of the environmental control system of the aircraft, as discussed by Chowdhury et al. [11] and Zhao et al. [12], solely due to the humidity of the ambient air. Considering the LH_2 conditioning heat exchangers will be utilising humid air either due to ambient conditions or due to the combustion products of H_2, water vapour condensation should be addressed.

2 Integrated Framework

In this analysis two parameters are considered that mainly affect the design space exploration of the integrated system, one related to engine specific design and another to the fuel conditioning system. From an engine point of view this is the specific thrust which dictates the size of the engine. Traditionally for a technology level minimizing the specific thrust is key to maximize propulsive efficiency, but in this case, the effect of the fuel conditioning integration and performance is examined across engine designs that provide the same amount of thrust but with different fan size. For the fuel conditioning, the key design parameter selected is the effectiveness of the heat exchanger. The hot and cold side pressure losses may be additional independent parameters for the design. Especially the hot side pressure losses for applications that utilize the whole engine core flow can significantly impact the system efficiency as discussed in Refs. [1], [3], and [4], however, in this case, since the heat exchanger is utilizing engine bleeds, the hot side pressure losses are considered to have a lower order impact on the overall engine performance.

The workflow for the design space exploration of the integrated system, is presented in Fig. 2. For the fuel conditioning system—engine performance simulations, the propulsion object oriented simulation software (PROOSIS) was used, a software widely adopted by academia and industry [13], while for the sizing and the off-design characterization of the heat exchanger a Cranfield University in-house tool is used.

At first the baseline Jet A-1 engine models are sized based on a three-point design approach for fixed thrust requirements across midcruise (MCR), top-of-climb (ToC), and end-of-runway (EoR) operating conditions. MCR is set as the design point (DP) where turbomachinery maps and nozzle areas are scaled, and then ToC and EoR are simulated at off-design (OD). The approach followed targets to maximize both the turbine entry temperature (TET) and overall pressure ratio (OPR) by matching a set of maximum temperature targets at EoR. In addition, for every design the bypass ratio (BPR) is optimized with the view of minimizing the specific fuel consumption at MCR, and the fan diameter is estimated at ToC.

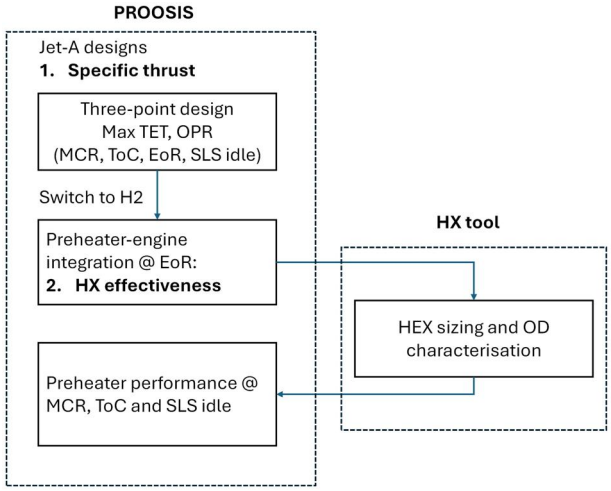


Fig. 2 Workflow overview

For simulating the engine at off-design, the duct and heat exchanger gas side pressure losses are set to vary according to the change in the corrected mass flow and the efficiency of the combustors according to the change in the combustor loading as discussed in Ref. [14].

Following the baseline model creation, the PHC conditioning module is integrated into the existing configurations, and the integrated model is then simulated at off-design for hydrogen. The design condition for the PHC is the EoR since at that condition the engine fuel flow reaches its peak value and therefore heat load requirement [10]. Pure hydrogen properties are used as detailed by NIST [2] and the combustion product properties for hydrogen have been obtained using NASA's CEA software [15]. The design requirements for the heat exchanger are then used in the heat exchanger sizing tool and the latter estimates the geometry and its off-design characteristics. These are updated to the integrated model and the MCR, ToC, and sea level static (SLS) idle operating points are simulated.

Finally, it is noted that the analysis herein assumes steady-state operating conditions dynamic response of the engine as well as the PHC module is not within the scope of this work and it would require a more detailed geometrical sizing of the components of the fuel conditioning system.

3 Heat Exchanger Sizing

In this section, the heat exchanger modeling and the overall sizing framework are presented, which comprises of three distinctive functionalities. The first is the design component, which involves the sizing of the heat exchanger geometry based on a set of requirements. The second is the rating component, which uses the geometry determined by the design tool and based on a set of input conditions estimates the performance. The third and final component is the regression tool, which creates lower-order correlations for the calculation of the heat exchanger effectiveness characteristics at off-design and are subsequently used within the propulsion system simulation models for the integrated assessment. Figure 3 summarizes the heat exchanger regression process using the described methodology.

3.1 Geometry. Several common fin configurations are presented in Fig. 4, including plain fin, louvered fin, offset strip fin, and wavy fin [16]. In the study, an offset strip fin configuration with specific dimensions (1/9–22.68) was selected for both the air and H_2 layers for a more compact heat exchanger design [17].

Figure 5 illustrates the general structure of plate-fin heat exchangers, particularly crossflow arrangement [18]. Although counterflow arrangement typically offers higher heat effectiveness compared to crossflow heat exchangers, the crossflow arrangement

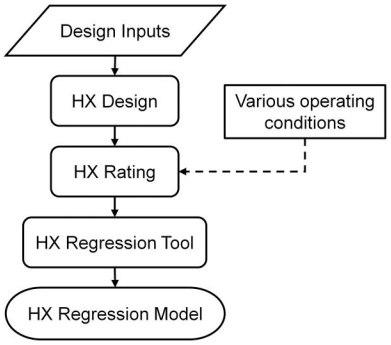


Fig. 3 Heat exchanger regression flowchart

was selected to simplify the integration process [18]. This is due to the intricate connection requirements for each layer in counterflow arrangement to prevent the mixing of fluids.

The effective number of transfer units (ε-NTU) method is applied to design the plate-fin heat exchanger, employing a thermal-hydraulic model to relate heat exchanger volume, heat transfer coefficients, and pressure drop, as described in Ref. [18]. Note that the fouling effect and longitudinal heat conduction influence are neglected in the study. Fouling is the degradation of heat exchanger performance due to the accumulation of residues on the heat exchanger surface. The longitudinal conduction effect is generally negligible in crossflow heat exchangers [18].

3.2 Heat Exchanger Modeling. The air-H_2 heat exchanger is incorporated to transfer the heat from the source air to the H2 line in the designed fuel conditioning system. Among various heat exchanger designs, the plate-fin heat exchanger was selected due to its notable compactness and high heat transfer capability, as size and weight are critical parameters for aviation applications. A plate-fin heat exchanger enables heat transfer between fluids using plates and finned chambers, which serve as secondary surfaces to increase the heat transfer area. The addition of fins induces fluid turbulence to enhance the local convective heat transfer coefficient.

In this design, the dimensionless parameters—the Colburn factor (j) and the Fanning friction factor (f)—are used to represent convective heat transfer performance and pressure drop. They are expressed as functions of Reynolds number (Re) and basic fin geometry parameters [16,18]. Manglik et al. [19] provided regression equations for the Colburn factor (j) and the Fanning Friction Factor (f) for offset strip fin configurations. In these equations, *c, b, x,* and *tf* denote pitch, height, length, and thickness of the fin, respectively, as depicted in Fig. 6 [16]. The prediction accuracy within 14% against the experimental data is reported in

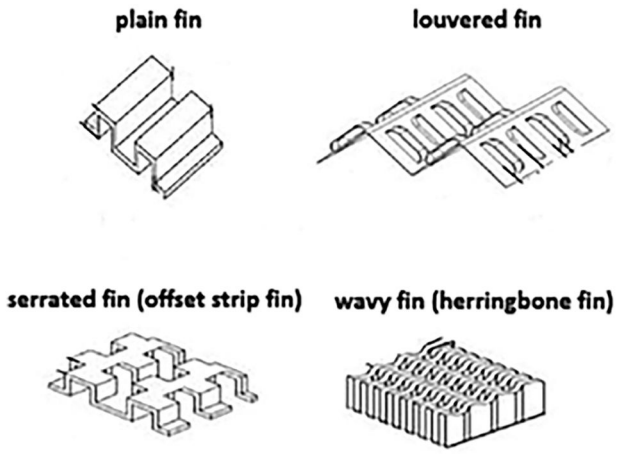


Fig. 4 Common fin configurations [16]

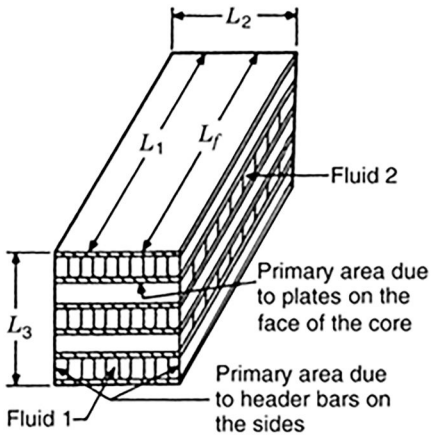


Fig. 5 Plate-fin heat exchanger—crossflow [18]

their study, representing a significant improvement over previous design works [19].

A plate-fin heat exchanger design tool is developed based on the described methodology Fig. 7, and it is structured into two main components: design and rating. The design component determines the geometrical configuration of the heat exchanger based on given design conditions and requirements. Then, the Rating component is used to evaluate the heat exchanger performance for given operating conditions based on the geometrical design data.

3.3 Heat Exchanger Regression Model. The integration of the developed plate-fin heat exchanger design tool into the overall system model poses challenges, including increased complexity and computational time. Hence, a regression model based on the ε-NTU method for plate-fin heat exchangers, incorporating an optimization algorithm, is developed to predict the heat exchanger's performance and mitigate these issues. The model is constructed using performance data collected within the heat exchanger's operating boundaries, ensuring accurate representation of its behavior under varying conditions [20].

The overall heat transfer conductance of the heat exchanger (UA) is expressed as follows, where G_{wall} represents the wall conductance, and subscripts hot and cold refer to the relevant side of the heat exchanger [18]

$$\frac{1}{\mathrm{UA}} = \frac{1}{\mathrm{UA}_{\mathrm{Hot}}} + \frac{1}{G_{\mathrm{wall}}} + \frac{1}{\mathrm{UA}_{\mathrm{Cold}}} \tag{1}$$

According to Nusselt number (Nu) and geometry correlations, the heat transfer conductance of each side of the heat exchanger can be expressed as follows, where λ represents the thermal conductivity,

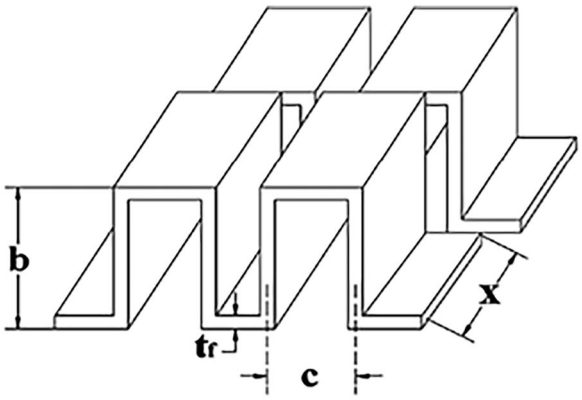


Fig. 6 Offset strip fin geometry [16]

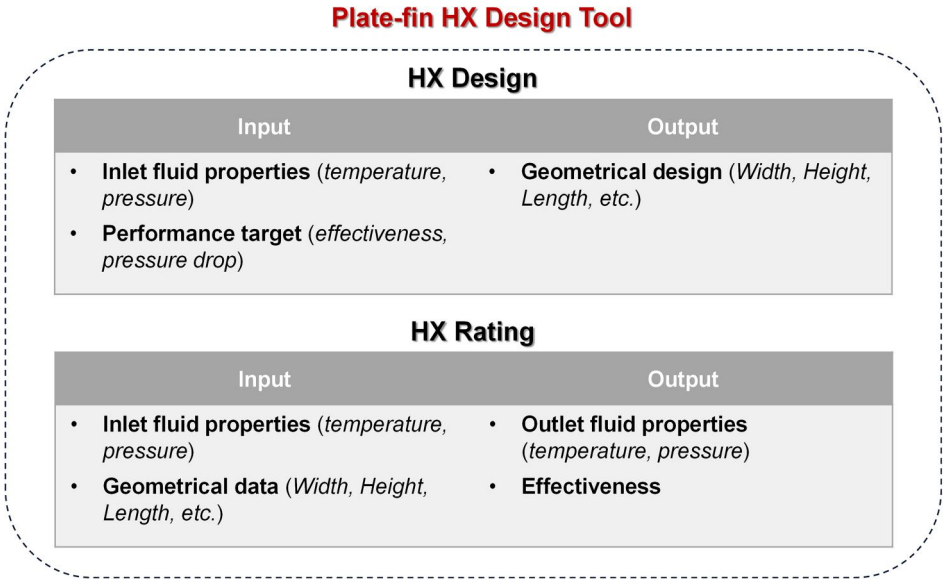


Fig. 7 Plate-fin heat exchanger design tool

A_{ex} the heat transfer area, and d_h the hydraulic diameter of each side of the heat exchanger

$$\mathrm{UA} = \frac{\mathrm{Nu} \cdot \lambda \cdot A_{ex}}{D_H} \tag{2}$$

where Nusselt number is a function of Reynolds number (Re) and Prandtl number (Pr)

$$\mathrm{Nu} = a \cdot \mathrm{Re}^b \cdot \mathrm{Pr}^c \tag{3}$$

The coefficients (a, b, and c) are optimized to have minimal heat transfer deviation against heat exchanger rating data over a given operating range. A differential Evolution algorithm is employed for optimization [20]. Subsequently the number of transfer units can be calculated via the UA and the minimum capacity for heat transfer, C, as shown in Eq. (4). Finally, the ε_{HX} is provided as a function of the NTU and the minimum to maximum capacities for heat transfer ratio of the two flows ($C^* = C_{min}/C_{max}$), which for cross-flow heat exchangers this is taken as discussed in Ref. [17] and presented in Fig. 8

$$\mathrm{NTU} = \frac{\mathrm{UA}}{C_{min}}, \text{ where, } C = W \times C_P \tag{4}$$

Having determined the heat exchanger effectiveness, the exit conditions can be estimated using the heat balance between the two streams as well as the definition of the heat exchanger effectiveness equations as shown in Eq. (5). As the flow conditions are averaged for the inlet and outlet conditions of the respective streams, the whole process is iterated until Eq. (5) is satisfied

$$\varepsilon_{HX} = \frac{C_{P,\mathrm{Cold}} \Delta T_{\mathrm{Cold}}}{C_{min}(T_{\mathrm{Hot,in}} - T_{\mathrm{Cold,in}})} = \frac{C_{P,\mathrm{Hot}} \Delta T_{\mathrm{Hot}}}{C_{min}(T_{\mathrm{Hot,in}} - T_{\mathrm{Cold,in}})} \tag{5}$$

The heat exchanger regression model results are shown in Fig. 9. It can be seen that the regression model is capable of predicting the heat transfer performance of the heat exchanger with reasonable accuracy while significantly reducing computational time.

4 Baseline Engine Cycles

As in the previous paper [10], the test case that is selected is targeting the short-to-medium range applications similar to the Airbus A320 or Boeing 737 family of aircraft with an entry into service 2030. The thrust requirements for such an application are adopted by another conceptual study as discussed by Alexiou et al. [21]. The engine configuration is a geared turbofan with a fixed

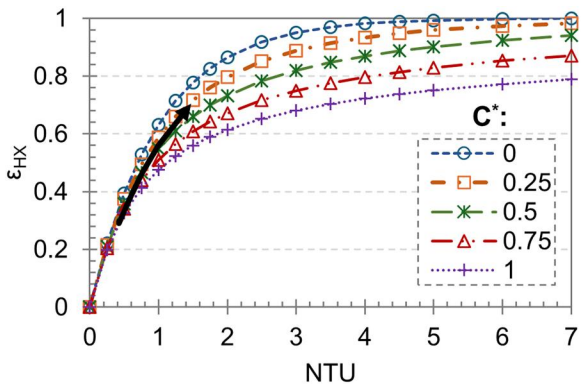


Fig. 8 ε_{HX} over NTU and C^* for cross flow heat exchangers [17]

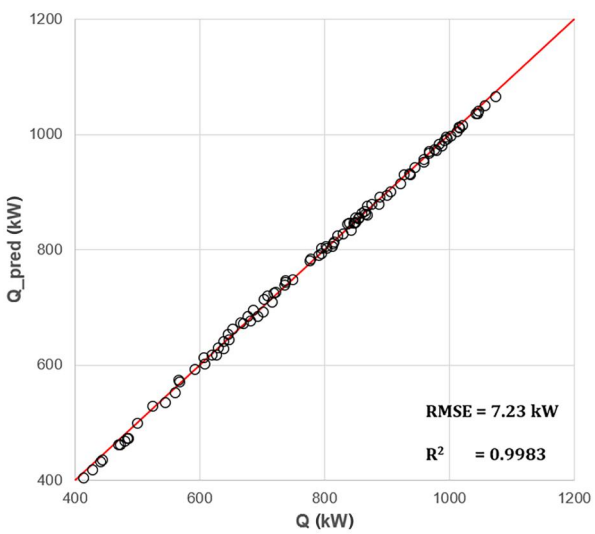


Fig. 9 Heat exchanger regression model result—heat transfer

bypass (BP) nozzle area. The engine thrust ratings for four representative points are presented in Table 1.

In this study several baseline engine cycles are created to represent designs of different specific thrust (SFN) requirements and herein, these are characterized by their design point fan pressure ratio (FPR). The engine cycles are sized according to the requirements of the three key operating conditions, MCR, ToC, and EoR, following a multipoint cycle design approach. The SLS idle setting will be considered subsequently for the performance assessment of the LH_2 conditioning system.

Four designs with varying FPR_{MCR} from 1.3 to 1.6 have been created and some key cycle parameters for MCR are presented in Table 2. Notably, higher FPR leads to higher specific thrust and more compact designs as observed by the decreasing fan diameter. In addition, lower specific thrust designs are characterized by higher fuel and energy-specific consumptions (SFC and ESFC, respectively) and higher BPR.

5 Preheater Stand-Alone On and Off Design Performance

Before addressing the integrated performance of the PHC module, an isolated scenario is examined to better understand the underlying behavior of the system. Two case studies are presented, the first is a parametric analysis of the design point performance of the PHC and the second an off-design analysis of the heat exchanger.

5.1 Hydrogen Combustion System Performance at Design. For this scenario the fuel flow requirement and delivery pressure for H_2 are considered constant and their values are assumed based on the rematched EoR performance of engine type 1 with H2 as fuel. Additionally, the secondary combustor (SC) exit temperature, pump isentropic efficiency are assumed constant and the inputs are summarized in Table 3. The heat exchanger effectiveness and the PHC feed mass flow ($W_{PHC,in}$) are varied between 0.3–0.8 and 1–5 kg/s, respectively.

For this analysis the resulting hydrogen delivery temperature ($T_{HX,Cold,out}$) is presented in Fig. 10 and the temperature at the exit of the hot side ($T_{HX,Hot,out}$) in Fig. 11. Considering a given value of ε_{HX}, with increasing WPHC, the cold side mass flow of the heat exchanger (HX) only slightly increases which is attributed to the slight increase in fuel flow of the SC and the constant main engine flow demand. Therefore, any increase in WPHC is directly driving an increase in heat transfer and as a result change in ΔT across either the hot or cold side. At low W_{PHC} the ΔT of the cold side is increasing and reaches a maximum value. Any increase in WPHC only reduces the ΔT of the hot side. This behavior is observed as the minimum capacity (C_{min}) for heat transfer in the HX changes between the hot side at low WPHC and the then cold side at higher values, as show in Fig. 12.

Choosing HX effectiveness has significant importance. High ε_{HX} suggests that higher ΔT can be achieved for the same mass flow or alternatively for a target $T_{HX,Cold,out}$ a heat exchanger with high effectiveness, requires less mass flow. Considering that the PHC module is driven by engine bleeds minimizing the mass flow requirement reduces the parasitic losses and the overall efficiency penalties of the engine. In addition, a low ε_{HX} could potentially limit the maximum $T_{HX,Cold,out}$ that can be achieved.

However, there are also cases where a high ε_{HX} may not be desirable. Considering the case with ε_{HX} of 0.8, the ΔT of the hot side is high enough that leads to a $T_{HX,Cold,out}$ of around 230 K (–43 °C). Even if it is assumed that the PHC is driven by dry air, the hot side of the heat exchanger operates with the exhaust gasses of the SC and since H_2 is burnt, there is a substantial quantity of water vapor in that gas that may condense and potentially freeze.

In order to check whether the set of conditions across the HX may lead water vapor to condense, the saturation temperature (TH_2O,sat) is calculated based on the partial static pressure of water vapor (p_{vapour}) for the flow conditions at the exit of the heat exchanger and the saturation properties of H_2O for that pressure as discussed in Ref. [22]. For a flow that comprises of dry air and water vapor, the partial static pressure for H_2O is calculated as shown in Eq. (6) according to static pressure of the mixture, the water/air ratio (WAR) of the flow, the molecular weight of dry air (M_{da}) and H_2O (MH_2O). The WAR is assumed based on the emission index for H2O, considering full stoichiometric combustion for H_2, and the fuel to air ratio (FAR) content of the flow. For 1 kg of hydrogen burnt, 8.937 kg of H_2O are produced.

For the designs considered here, the ones with ε_{HX} 0.8 dictate a significant temperature drop across the hot side, since for these conditions the exit temperature is below the saturation point of water vapor at 316 K:

Table 1 Thrust requirements across design operating points

Operating point	MCR (DP)	ToC	EoR	SLS idle
FN (kN)	20.1	24.3	94.7	14.4
Mn (–)	0.78	0.78	0.25	0
Altitude (kft)	35	35	0	0
dT_{ISA} (K)	0	+10	+15	0

Table 2 Jet A-1 baseline model results at MCR

Engine type		1	2	3	4
FPR	–	1.3	1.4	1.5	1.6
SFC	g/(kN·s)	13.79	14.03	14.31	14.62
ESFC	W/N	595	605	617	630
OPR	–	43.97	43.53	42.68	41.83
TET	K	1557	1547	1541	1531
W_{inlet}	kg/s	288.0	229.7	194.3	170.7
WF	kg/s	0.2772	0.2820	0.2877	0.2938
BPR	–	17.63	13.47	10.98	9.24
SFN	m/s	69.8	87.5	103.5	117.7
D_{Fan}	m	2.07	1.85	1.71	1.61

Table 3 Example inputs

Parameter	Units	Value
WF	kg/s	0.308
$P_{HX,Cold,out}$	bar	88
$T_{HX,Hot,in}$	K	1000
$P_{PHC,in}$	bar	1.25
$T_{PHC,in}$	K	323
$\eta_{is,pump}$	–	0.5
ε_{HX}	–	0.3–0.8
$W_{PHC,in}$	kg/s	1–5

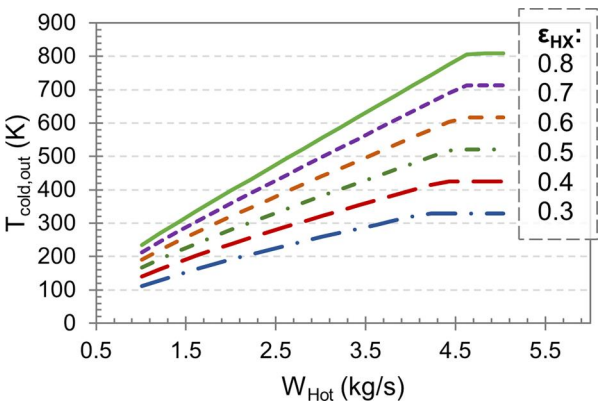


Fig. 10 $T_{Cold,out}$ as a function of W_{Hot} and ε_{HX}

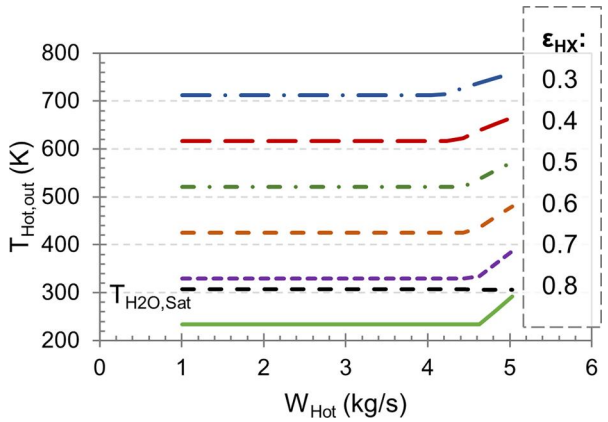


Fig. 11 $T_{Hot,out}$ as a function of W_{Hot} and ε_{HX}

$$p_{vapour} = \frac{p_{mixture}\,WAR}{M_{water}/M_{dry,air} + WAR} \tag{6}$$

5.2 Hydrogen Combustion System Off-Design Case Study. In this case, a heat exchanger design is considered and its off-design performance is calculated and addressed. From the previous parametric study, the design selected corresponds to a ε_{HX} of 0.3 and WPHC of 2.75 kg/s, which delivers the cold flow at a $T_{Cold,out}$ at 250 K. Based on these design conditions, the geometry is calculated, and then a sweep of W_{Cold} and W_{Hot} for the same inlet pressures and temperatures is performed. The resulting ε_{HX} is presented in Fig. 13.

This shows great variation in any other condition, and considering that the MCR, ToC, and SLS idle would require considerably lower

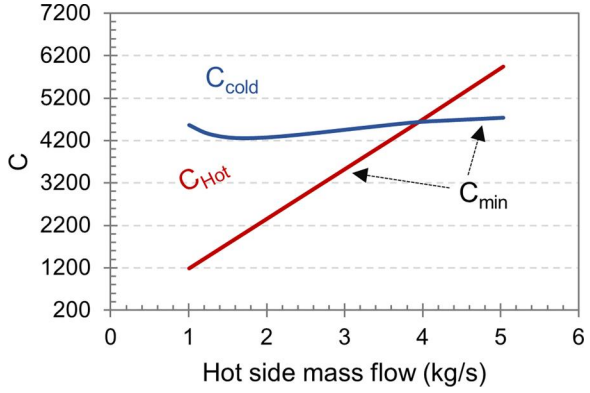


Fig. 12 C_{Cold} and C_{Hot} over W_{PHC} for 0.3 ε_{HX}

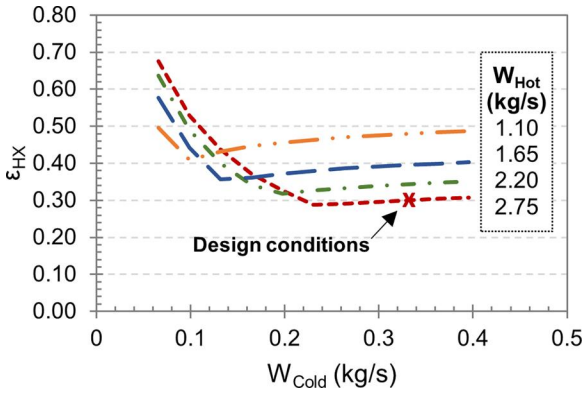


Fig. 13 ε_{HX} as a function of W_{Cold} and W_{Hot}

fuel flows than the EoR, it is expected that the ε_{HX} will be higher at these conditions. More precisely, at constant W_{Hot}, when the cold side is C_{min}, increasing the cold side mass flowrate leads to an increase in both C_{min} and the UA. However, the NTU decreases because C_{min} increases more significantly than UA, as shown in Eq. (4). Additionally, the C^* approaches unity as the cold side mass flowrate increases. As a result, the ε_{HX} decreases due to these effects, as depicted in Fig. 13. This trend changes once the hot side conditions dictate the C_{min}. Since the hot side mass flowrate remains fixed, the ε_{HX} becomes relatively stable, slight increment is caused by the changes in C^*. Overall, high ε_{HX} is desirable to minimize bleed flow and parasitic engine losses, but there needs to be careful control in order to avoid excessive temperature drop at the hot side.

6 Hydrogen Combustion System Integrated Performance

6.1 Integrated Model Set-Up. To assess the integrated performance of the system, the PHC module is then integrated with the baseline engine model, as shown in Fig. 14. The heat exchanger and PHC nozzle areas are calculated at EoR, which is the design case of the integrated model, and at any other operating condition the sized geometry of these components is used to assess the performance.

For on-design point simulation, the following handles are considered:

- Thrust requirement
- $T_{HX,Cold,out}$ 250 K (H_2 delivery temperature)
- $P_{H2,delivery}$ is set twice the $P_{HPC,exit}$
- $T_{HX,Hot,in}$ 1000 K

For off design simulations, the same handles are used as described above, only in this case, the valve installed upstream of the SC is varied so that the mass flow continuity in the scaled nozzle is satisfied. Here this is simulated as a component that imposes pressure losses in the flow, at the design case it is fully open and at

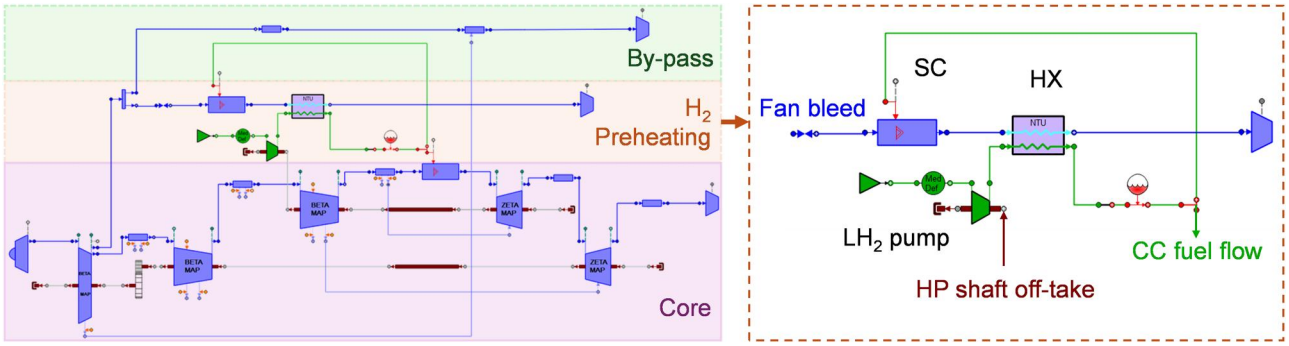


Fig. 14 PHC integrated engine model in PROOSIS

Table 4 Integrated model additional considerations

Parameter	Value
$T_{pump,in}$	21 K
$P_{pump,in}$	1.5 bar
$P_{pump,out}$	$2 \times P_{HPC,exit}$
$(dP/P_{in})_{HX,Hot}$	2%
$(dP/P_{in})_{HX,Cold}$	0.1%

any other condition variable. Moreover, additional conditions are imposed on the $T_{HX,Hot,in}$ with the view of avoiding water vapor condensation at the exhaust of the hot side of the heat exchanger while minimizing the PHC mass flow requirement. To achieve this, the objective is to maximize $T_{HX,Hot,in}$ (up to 1000 K) while considering the following conditions:

- $T_{HX,Hot,out} \geq T_{H2Osat}$
- If $T_{HX,Hot,out} < T_{H2Osat}$ then minimize $T_{HX,Hot,out} - T_{H2Osat}$ to reduce the condensation effect, or until $T_{HX,Hot,in}$ is 330 K. The later is imposed to avoid solutions that dictate high mass flows bled from the engine.

Furthermore, the H_2 conditions at the pump inlet are assumed to be discussed by Brewer [1], the pump pressure ratio is dependent on the HPC delivery pressure, the heat exchanger pressure losses for both sides are set with the view of acquiring representative flow velocities on both sides. The inputs discussed are summarized in Table 4.

6.2 Hydrogen Combustion System Performance Comparison With and Without Temperature Control on the Hot Side. From the design space exploration for the PHC, a case is selected and discussed in detail to demonstrate the different control over the $T_{HX,Hot,out}$. For that purpose, engine type 1 is used and the PHC is sized for 0.5 ε_{HX}. The performance of this PHC configuration is presented in Table 5, for two scenarios. In the first, $T_{HX,Hot,in}$ is maximized at 1000 K at all operating conditions as suggested by previous studies [10], and in the second, its control is applied as proposed in this paper.

Table 5 PHC performance comparison with and without exhaust condensation control

	MCR	ToC	EoR	SLS idle
		Maximum $T_{Hot,in}$		
ε_{HX}	0.80	0.76	0.50	0.95
$T_{Hot,in}$ (K)	1000	1000	1000	1000
$T_{Hot,out}$ (K)	220	260	525	81
$T_{Cold,in}$ (K)	31.2	32.0	41.6	28.2
$T_{Cold,out}$ (K)	250	250	250	250
FAR (–)	0.696%	0.683%	0.636%	0.673%
W_{Hot} (kg/s)	0.326	0.418	1.660	0.100
W_{Cold} (kg/s)	0.1012	0.1235	0.3223	0.0360
PHC valve opening	58%	61%	100%	97%
A_{pre} (m^2)	0.0088	0.0088	0.0088	0.0088
T_{satH2O}	293	294	320	317
	Variable $T_{Hot,in}$ for condensation control			
ε_{HX}	0.63	0.69	0.50	0.73
$T_{Hot,in}$ (K)	728	868	1000	330
$T_{Hot,out}$ (K)	289	292	525	243
$T_{Cold,in}$ (K)	31.2	32.0	41.6	28.2
$T_{Cold,out}$ (K)	250	250	250	250
FAR (–)	0.415%	0.543%	0.636%	0.032%
W_{Hot} (kg/s)	0.610	0.552	1.660	1.139
W_{Cold} (kg/s)	0.1018	0.1238	0.3223	0.0358
PHC valve opening	77%	70%	100%	105%
A_{pre} (m_2)	0.0088	0.0088	0.0088	0.0088
T_{satH2O} (K)	289	292	320	271
	Comparative differences with against without control			
ESFC	0.6%	0.3%	0.0%	–0.7%

For the first case, it is evident that the ε_{HX} is significantly higher at MCR, ToC, and SLS idle than its design value at EoR. This in turn leads to a high ΔT across the hot side of the HX and results in an exit temperature well below the saturation conditions of water vapor, not only for SLS idle but also for MCR and ToC. The variation observed in the TsatH2O is mainly driven by the change in ambient pressure and fan operating point rather than the change in the FAR of the flow. In all operating conditions, it can also be observed that the variation in valve opening, which suggests that in all cases there is adequate source pressure for the PHC.

In the second case, the $T_{HX,Hot,in}$ is changed significantly across all operating conditions but for EoR. The variance now in ε_{HX} at MCR, ToC, and SLS idle is lower but at a cost of increased PHC mass flow requirement (as seen by the W_{Hot}). At MCR and ToC the $T_{HX,Hot,out}$ matches that of the T_{satH2O}, however, not at SLS idle, due to the fact that the $T_{HX,Hot,in}$ is limited to 330 K. As the $T_{HX,Hot,in}$ becomes lower, the FAR and the associated WAR of the exhaust gases also decreases and these mechanisms drives a small decrease in T_{satH2O}. In addition to that, the decrease in available ΔT over the hot side of the HX dictates a tenfold increase in mass flow, compared to the first case, and cannot be supported by the bypass duct due to low source pressure as seen by the valve opening. Therefore, this design suggests that during SLS idle, the PHC needs to be assisted by auxiliary means of source air and is likely that water vapor will be condensing and may form ice at the exhaust of the PHC.

Between the two cases, the one that controls the $T_{HX,Hot,out}$ compared to the other, shows a small penalty in engine efficiency of 0.6% and 0.3% at MCR and ToC, respectively. This mainly driven by the increase PHC mass flow requirement and SC fuel flow.

6.3 Integrated Model Design Space Exploration. The design space exploration of PHC integration is mainly focused on the effect of utilizing different heat exchanger designs across all engine types and in particular at design the ε_{HX} is varied between 0.3 and 0.6. For the discussion that will follow, the heat exchanger designs will be characterized by their design effectiveness (at EoR). As demonstrated from the previous test case, the objective herein is to identify requirements and limitations for the engine—PHC. Therefore, the results are focused on the MCR and SLS idle conditions.

Starting with the MCR performance, the temperature difference between the $T_{HX,Hot,out}$ and the T_{satH2O} is presented in Fig. 15 and the valve opening in Fig. 16. Across all engine types the 0.3 ε_{HX} designs and the combination of types 1 and 0.4 ε_{HX} allow for adequate margin over the condensation region at the exhaust of the PHC. In every other combination, a limit in the $T_{HX,Hot,in}$ is imposed and in the cases of high specific thrust (types 3 and 4)—effectiveness, the margin is exceeded. This also cascades to high PHC mass flow requirements, as shown in plot (*a*) of Fig. 17, which cannot be accommodated based on the source conditions and the sized nozzle as shown by the required valve opening.

The ESFC difference to the baseline Jet A performance is shown in Fig. 18. Across all combinations but for the 0.6 ε_{HX} designs the

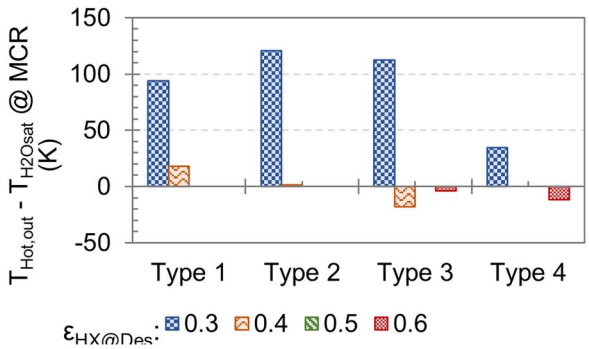


Fig. 15 Condensation temperature margin at MCR over varying heat exchanger designs and engine types

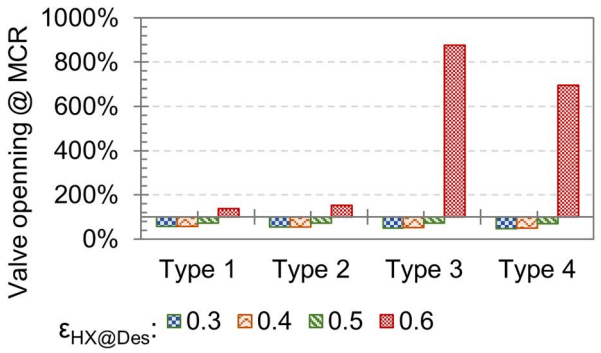


Fig. 16 Valve opening at MCR over varying heat exchanger designs and engine types

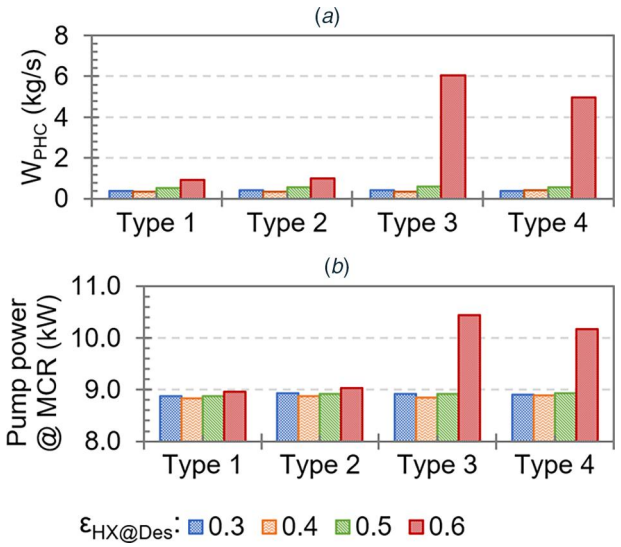


Fig. 17 PHC mass flow (*a*) and pump power (*b*) requirements at MCR over varying heat exchanger designs and engine types

ESFC is increased by approximately 2% with little variation over the heat exchanger design. The 0.6 ε_{HX} is significantly penalizing the performance of the baseline cycle due to the significant increase in WPHC bleed that is required to minimize the condensation temperature margin and has also a cascading effect in pump power requirement due to the increased fuel flow, as shown by plot (*b*) of Fig. 17. In Fig. 19, the ESFC difference of the integrated models with

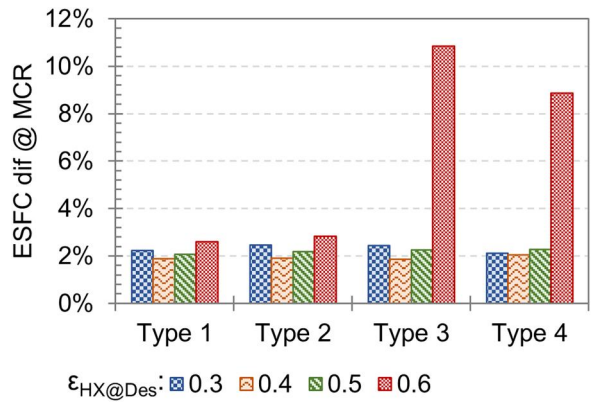


Fig. 18 ESFC difference compared to the respective baseline engine performance over varying heat exchanger designs and engine types

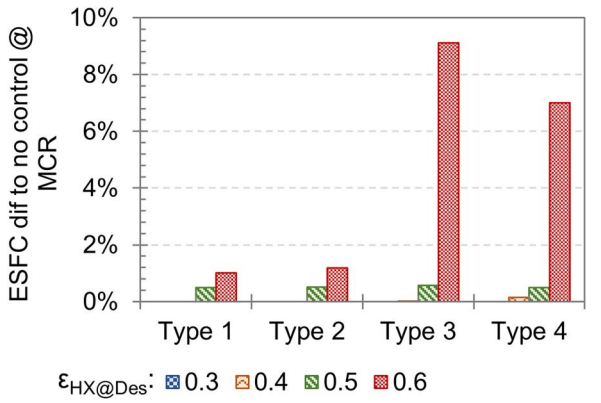


Fig. 19 ESFC difference with and without $T_{HX,Hot,out}$ control

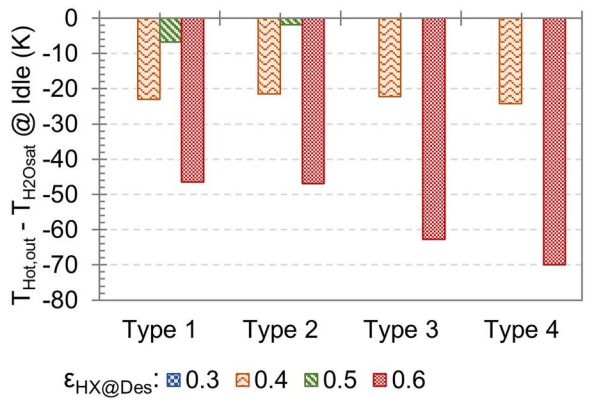


Fig. 20 Condensation temperature margin at SLS idle over varying heat exchanger designs and engine types

and without $T_{HX,Hot,in}$ control is presented. The differences become more significant for the designs with higher ε_{HX} designs of up to 9%.

In a similar manner, the condensation temperature margin for the SLS idle is presented in Fig. 20 and the valve opening in Fig. 21. The 0.3 ε_{HX} across all engine types and the 0.5 on high specific thrust engine types can adequately provide control so that condensation conditions at the HX exhaust are avoided. The 0.4 and 0.6 designs, however, are more limited in that respect. In addition, for all but the 0.3 i_{HX} designs, there source pressure from the BP is not sufficient to drive the PHC module. Finally, the volume of the heat exchanger is presented in Fig. 22. Higher ε_{HX} designs occupy bigger volume due to the increase in heat exchange area required. Heat exchangers

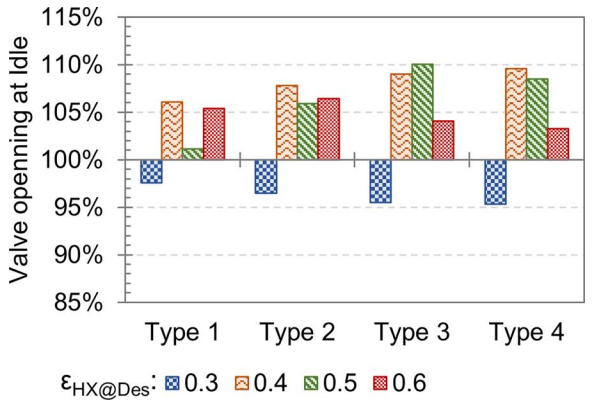


Fig. 21 Valve opening at SLS idle over varying heat exchanger designs and engine types

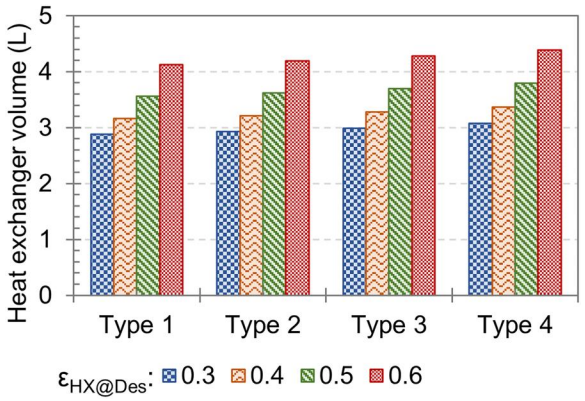


Fig. 22 Heat exchanger volume across the design space

designed with the same ε_{HX} have marginally bigger volume when used at higher specific thrust engines, which is attributed to the increased fuel flow and associated heat requirement.

Overall, it can be concluded that lower ε_{HX} designs are desirable, as they can allow for adequate control over the exhaust temperature of the PHC, avoiding conditions where condensation occurs, and can adequately be supplied from air sourced from the BP duct without the support of auxiliary systems.

7 Conclusions

The paper introduced a methodology for the integrated assessment of engine—LH_2 conditioning system with focus on the heat exchanger sizing and off-design performance. In addition, water vapor condensation was identified on these systems across key operating conditions of the engine and a mitigation strategy was proposed. A preliminary exploration of the operational envelope of a kerosene-based civil turbofan engine retrofitted with a LH_2 preheater system, considering various heat exchanger designs. The study concludes on the following points:

Considering that the inlet temperature of the hot side of the heat exchanger is constrained by the thermal limits of its material and that the gasses have a considerable amount of water vapor, heat exchanger designs that enable high temperature drop may potentially lead to conditions at the exhaust where the water vapor condenses and freezes. This could create significant operability problems related to corrosion or the blocking of the PHC module.

The heat exchanger is designed according to EoR conditions due to the highest thermal input requirements across the flight envelope. During other conditions like MCR and SLS idle where these thermal loads are lower, the heat exchanger allows for higher effectiveness. To mitigate the formation of water at the heat exchanger exhaust, the SC delivery temperature should be regulated at the expense of higher bleed flow demand from the engine.

The design space exploration showcased that heat exchangers with high effectiveness at design, e.g., for the cases of 0.5 and 0.6, fail to regulate the hot side outlet conditions to avoid water condensation both at SLS and MCR. At the same time, as the bleed flow requirement is increased at these conditions, the source pressure is not adequate to drive the PHC unit, and the latter should be supported by other pneumatic aircraft systems.

Lower effectiveness designs can mitigate water condensation at the heat exchanger and at the same time, can be fully supported by the bypass duct delivery conditions and are more compact. It is acknowledged, however, that the pressure margins at SLS idle are limited and therefore at these and lower power setting conditions the PHC may need to be supported by auxiliary aircraft systems.

Based on the new control conditions introduced, the temperature delivery requirements of the SC vary significantly throughout the critical operating points, and therefore, this dictates the emerging requirements for its design. At a later stage, limitations considering the SC can be introduced to the existing analysis to further narrow the design space and identify feasible solutions.

Although heat exchangers with higher effectiveness minimize the hot flow requirement at EoR, at MCR due to the water vapor condensation mitigation strategy used, all designs, but for the 0.6 case, seem to show marginal differences in energy consumption.

Engine designs with higher specific thrust require more fuel flow compared to lower ones and therefore require more bleed flow from the engine to accommodate the higher heat load requirement. This results in heat exchangers with marginally bigger size.

Acknowledgment

The authors are grateful to Rolls-Royce plc for its guidance during the project and Empresarios Agrupados for their continuous support with PROOSIS. The authors confirm that the data supporting the findings of this study are available within the article.

Funding Data

- Innovate UK (Project Reference No. 10039770 (LH2GT); Funder ID: 10.13039/501100006041).

Nomenclature

A_{ex} = heat transfer area
B = fin height
BP = bypass
BPR = bypass ratio
c = fin pitch
C = capacity for heat transfer
C^* = minimum-to-maximum capacity for heat transfer
CEA = chemical equilibrium with applications
CP = specific heat capacity
D = diameter
DP = design point
EoR = end-of-runway
ESFC = energy-specific fuel consumption
f = fanning friction factor
FAR = fuel-to-air ratio
FN = net thrust
FPR = fan pressure ratio
G_{wall} = wall conductance
HX = heat exchanger
ISA = international standard atmosphere
j = Colburn factor
LH_2 = liquid hydrogen
M = molecular weight
MCR = midcruise
Mn = Mach number
NIST = National Institute of Standards and Technology
NTU = number of transfer units
Nu = Nusselt number
OD = offdesign
OPR = overall pressure ratio
p = static pressure
P = total pressure
PHC = parallel hydrogen combustion system
Pr = Prandtl number
PROOSIS = propulsion object oriented simulation software
Re = Reynolds number
SC = secondary combustor
SFC = specific fuel consumption
SFN = specific thrust
SLS = sea-level static
T = total temperature
t_f = fin thickness
TET = turbine entry temperature
ToC = top-of-climb
UA = overall heat transfer conductance

W = mass flow rate
WAR = water/air ratio
WF = fuel flow rate
x = fin length
ε = effectiveness
η = efficiency
λ = thermal conductivity

Subscripts

da = dry air
H = hydraulic
is = isentropic
sat = saturation

References

[1] Brewer, D., 1990, *Hydrogen Aircraft Technology*, CRC Press, New York.
[2] NIST, 2020, "Thermophysical Properties of Fluid Systems," NIST, accessed Oct. 30, 2020, https://webbook.nist.gov/chemistry/fluid/
[3] Patrao, A. C., Jonsson, I., Xisto, C., Lundbladh, A., and Grönstedt, T., 2024, "Compact Heat Exchangers for Hydrogen-Fueled Aero Engine Intercooling and Recuperation," Appl. Therm. Eng., **243**, p. 122538.
[4] Abedi, H., Xisto, C., Jonsson, I., Grönstedt, T., and Rolt, A., 2022, "Preliminary Analysis of Compression System Integrated Heat Management Concepts Using LH2-Based Parametric Gas Turbine Model," Aerospace, **9**(4), p. 216.
[5] Palmer, C. J., 2024, "Hydrogen Fuel Vaporiser," US Patent No. EP 3978738 B1.
[6] Tacconi, J., and Grech, N., 2023, "Advanced Hydrogen Cycles to Help Decarbonize the Aviation Industry. Part 1: Development of Simulation & Modeling Toolsets," ASME Paper No GT2023-103505.
[7] Huete, J., Nalianda, D., and Pilidis, P., 2021, "Propulsion System Integration for a First-Generation Hydrogen Civil Airliner?," Aeronaut. J., **125**(1291), pp. 1654–1665.
[8] Saias, C., Roumeliotis, I., Goulos, I., Pachidis, V., and Bacic, M., 2022, "Assessment of Hydrogen Fuel for Rotorcraft Applications," Int. J. Hydrogen Energy, **47**(76), pp. 32655–32668.
[9] Rischmüller, U., Johannes, C., Lessis, A., Egerer, P., and Hornung, M., 2024, "Conceptual Design of a Hydrogen-Hybrid Dual-Fuel Regional Aircraft Retrofit," Aerospace, **11**(2), p. 123.
[10] Rompokos, P., Kyritsis, V., Mourouzidis, C., and Roumeliotis, I., 2024, "Assessment of a Liquid Hydrogen Conditioning System for Retrofitting on Kerosene Designed Turbofan," ASME Paper No. GT2024-121997.
[11] Chowdhury, S. H., Ali, F., and Jennions, I. K., 2023, "Development of a Novel Ground Test Facility for Aircraft Environmental Control System," ASME J. Therm. Sci. Eng. Appl., **15**(8) p. 081012.
[12] Zhao, H., Hou, Y., Zhu, Y., Chen, L., and Chen, S., 2009, "Experimental Study on the Performance of an Aircraft Environmental Control System," Appl. Therm. Eng., **29**(16), pp. 3284–3288.
[13] EA Internacional, 2023, "PROOSIS—Propulsion Object-Oriented Simulation Software," EA Internacional, accessed Dec. 10, 2023, https://www.ecosimpro.com/products/proosis/
[14] Walsh, P., and Fletcher, P., 2004, *Gas Turbine Performance*, Second, Wiley, Blackwell Science, Oxford, UK.
[15] Gordon, S., and McBride, B., 1994, "Computer Program for Calculation Complex Chemical Equilibrium Compositions and Applications. Part 1 Analysis," NTRS - NASA Technical Reports Server, Cleveland, OH, accessed Dec. 6, 2023, https://ntrs.nasa.gov/citations/19950013764
[16] Guo, K., Zhang, N., and Smith, R., 2015, "Optimisation of Fin Selection and Thermal Design of Counter-Current Plate-Fin Heat Exchangers," Appl. Therm. Eng., **78**, pp. 491–499.
[17] Kays, W. M., and London, A. L., 1998, *Compact Heat Exchangers*, 3rd ed., Krieger Publishing Company, Malabar, FL.
[18] Shah, R. K., and Sekulić, D. P., 2003, *Fundamentals of Heat Exchanger Design*, Wiley, Hoboken, NJ.
[19] Manglik, R. M., and Bergles, A. E., 1995, "Heat Transfer and Pressure Drop Correlations for the Rectangular Offset Strip Fin Compact Heat Exchanger," Exp. Therm. Fluid Sci., **10**(2), pp. 171–180.
[20] Blank, J., and Deb, K., 2020, "Pymoo: Multi-Objective Optimization in Python," IEEE Access, **8**, pp. 89497–89509.
[21] Alexiou, A., Aretakis, N., Kolias, I., and Mathioudakis, K., 2021, "Novel Aero-Engine Multi-Disciplinary Preliminary Design Optimization Framework Accounting for Dynamic System Operation and Aircraft Mission Performance," Aerospace, **8**(2), p. 49.
[22] Roumeliotis, I., and Mathioudakis, K., 2006, "Analysis of Moisture Condensation During Air Expansion in Turbines," Int. J. Refrig., **29**(7), pp. 1092–1099.

DSPACE

https://dspace.org/

Integrated design and operation assessment of a preheating system for liquid hydrogen fueled engines

Rompokos, Pavlos; Kang, Sangkeun; Roumeliotis, Ioannis

2026-08
American Society of Mechanical Engineers (ASME)
https://doi.org/10.1115/1.4071241
Rompokos P, Kang S, Roumeliotis I. (2026) Integrated design and operation assessment of a preheating system for liquid hydrogen fueled engines. Journal of Engineering for Gas Turbines and Power, Volume 148, Issue 8, August 2026, Article number 081015

Downloaded from a DSpace repository. https://dspace.org/